International Journal of Pediatric Otorhinolaryngology 129 (2020) 109788

Contents lists available at ScienceDirect

International Journal of Pediatric Otorhinolaryngology

journal homepage: www.elsevier.com/locate/ijporl

Surgical mapping of middle ear cholesteatoma with fusion of computed tomography and diffusion-weighted magnetic resonance images: Diagnostic performance and interobserver agreement

Sunil Dutt Sharma, Andrew Hall, Anthony C. Bartley, Paul Bassett, Arvind Singh, Ravi K. Lingam*

Department of Radiology & Otolaryngology, Northwick Park Hospital, Watford Road, Harrow, HA1 3UJ, London, United Kingdom

ARTICLE INFO

Keywords:
Cholesteatoma
Magnetic resonance imaging
Diffusion weighted MRI
Computed tomography

ABSTRACT

Objective: To assess the diagnostic performance in detecting primary cholesteatoma at various anatomical subsites using Computed Tomography (CT), Diffusion-weighted Magnetic Resonance Imaging (DWMRI) and Fusion of CT and DWMRI (Fusion CT-MRI) images.

Study design: A retrospective study of 22 children identified from a prospective database of surgically treated cholesteatoma cases over a five year period. All cases underwent pre-operative CT, non-echo planar DWMRI and Fusion CT-DWMRI, and with clearly documented surgical findings. For each imaging modality, two radiologists scored for the presence or absence of cholesteatoma with confidence levels at different anatomical subsites. The radiologists were blinded to the surgical findings to which their findings were compared.

Setting: Large Teaching Hospital in London.

Patients: 22 children with cholesteatoma confirmed surgically.

Intervention: CT, DWMRI imaging and fusion CT-MRI.

Main outcome measure: Diagnostic performance of subsite localisation of cholesteatoma by CT, DWMRI and fusion CT-MRI imaging with intra-operative findings.

Results: Twenty-two patients were included (12 women and 10 men). The median age of patients was 11 years. When considering all subsites combined, the result for all imaging methods suggested 'good' agreement between both observers. When all subsites were examined together, all methods had relatively high sensitivity values (87% for CT vs 84% for DWMRI vs 85% for fusion CT-DWMRI). Specificity was highest with fusion CT-DWMRI (46% for CT vs 76% for DWMRI vs 97% for fusion CT-DWMRI), as was accuracy (66% for CT vs 80% for DWMRI vs 91% for fusion).

Conclusions: Our study has demonstrated that fusion CT-DWMRI is superior to DWMRI or CT separately in localizing cholesteatoma at various middle ear cleft subsites and bony relations, making it a valuable tool for surgical planning.

1. Introduction

The role of imaging in cholesteatoma continues to gather momentum with excellent middle ear cleft bony detail provided by high resolution computed tomography (CT) and high diagnostic performance for cholesteatoma detection and mapping by diffusion-weighted magnetic resonance imaging (DWMRI) [1,2]. High resolution CT of the temporal bones is the initial imaging modality of choice for primary middle ear cholesteatoma prior to surgery. CT not only depicts the disease but also its extent and bony complications as well as the relationship to key anatomical landmarks and abnormal anatomical variants, such as a prominent sigmoid sinus or aberrant course of facial nerve, which aid in surgical planning. It is, however, poor at differentiating cholesteatoma from co-existing inflammation and fluid and hence limited in defining the extent of true disease in a completely opacified middle ear cleft [2,3]. In terms of its use for detecting post-operative cholesteatoma, it has suboptimal performance with a reported sensitivity of 42.9%, specificity of 48.3% and positive predictive value of 28.6% [4].

More recently, in the post-operative context, non-echo-planar (non-EPI) DWMRI has become the imaging of choice for detecting cholesteatoma, partly due to its excellent ability to differentiate granulation

* Corresponding author.
E-mail addresses: sunilsharma@doctors.org.uk (S.D. Sharma), andyhall07@googlemail.com (A. Hall), dr_acbartley@yahoo.com.au (A.C. Bartley), paul@statsconsultancy.co.uk (P. Bassett), arvind.singh1@nhs.net (A. Singh), ravi.lingam@nhs.net (R.K. Lingam).

https://doi.org/10.1016/j.ijporl.2019.109788
Received 15 September 2019; Received in revised form 16 November 2019; Accepted 16 November 2019
Available online 20 November 2019
0165-5876/

tissue from cholesteatoma [1,5–9]. Non-EPI DWMRI has been shown to detect cholesteatoma down to 2 mm in size with a sensitivity of 91% and specificity of 92% with non-EPI DWMRI [1].

The use of fusion of CT and DWMRI (Fusion CT-DWI) combines the advantages of CT (good bony anatomical detail) with that of DWMRI (accurately characterizing and detecting cholesteatoma), and has been shown to enhance localisation of middle ear cleft cholesteatoma detected on DWMRI [10–12]. The aim of this study was to compare the diagnostic performance and interobserver agreement of CT, DWMRI and fusion CT-DWMRI for detecting primary cholesteatoma at various specific middle ear cleft anatomical subsites.

2. Materials and methods

Ethical approval for the study was obtained from our institution. A retrospective review of 22 patients identified from a prospective database of surgically treated cholesteatoma cases, over a 5-year period, who underwent pre-operative high resolution CT temporal bone and non-echo planar DWMRI, as well as surgical intervention, was performed. Cases where there was greater than 1 year duration between imaging and surgical intervention were excluded. The median (gap and range) between imaging and surgical intervention was assessed.

Non–contrast enhanced CT was performed on a 16-row multi-detector CT scanner (Phillips Brilliance; Phillips, Amsterdam, The Netherlands). High resolution helical scan acquisition with bone algorithm was performed with 0.67 mm thick axial slices and 0.67 mm thick coronal reformats (perpendicular to the hard palate) obtained. DWMRI was performed on a 1.5-T superconductive unit (Magnetom Avanto; Siemens Medical Solutions, Erlangen, Germany) using standard Head Matrix coil and coronal 2-mm thick non–echoplanar HASTE DWMRI sequence were acquired (TR 1600 ms; TE 113 ms; matrix 134 x 192; field of view 220 × 220 mm; b factors 0 and 1000 s/m2) using two b values: b0 and b1000).

Following acquisition, fusion of CT and DWMRI b1000 images (Fusion CT-DWMRI) was performed using TeraRecon Inc., Aquarious software (Version 4.4) on the Picture Archiving and Communication System (PACS) (Sectra, Linkoping, Sweden). The acquired axial CT scan volume and coronal b1000 images were selected for fusion. Automatic multiplanar registration of the images was performed by the software followed by manual fine-tuning by the senior radiologist (RL), taking approximately 15–20 min per scan. The fused CT-DWMRI images were saved onto PACS for subsequent blinded review analysis.

Two radiologists (RL and AB), blinded to each other's assessments and to the surgical findings, then assessed each form of imaging separately (CT, DWMRI and fusion CT-DWMRI) and scored their confidence in identifying cholesteatoma in different anatomical subsites (anterior epitympanum, aditus, facial recess, sinus tympani, eustachian tube orifice, facial nerve canal involvement, hypotympanum, disease lateral to ossicles and disease medial to ossicles, mastoid). The anatomical subsite of ‘mastoid’ included the antrum. The location of ‘aditus’ (including the posterior epitympanum) on DWMRI was approximated using the lateral semicircular canal. There were limitations in identifying the smaller anatomical subsites on DWMRI such as the facial recess, sinus tympani, and anterior epitympanum, so their location was approximated using anatomical landmarks such as the lateral semicircular canal, floor of the external canal, and scutum. Fig. 1 demonstrates cholesteatoma in Prussak's space on DWMRI, and Fig. 2 demonstrates cholesteatoma in the sinus tympani on DWMRI.

A scale of 1–5 was used (1 = cholesteatoma definitely absent, 2 = probably absent, 3 = possibly present, 4 = probably present to 5 = cholesteatoma definitely present). A confident CT diagnosis of cholesteatoma in the subsite (score 5) was made by the presence of soft tissue with local bony and ossicular erosion whereas a confident diagnosis for absence of cholesteatoma (score 1) was made with the absence of soft tissue in the subsite. A borderline diagnosis score of 3 referred to abnormal soft tissue in the subsite but not associated with bone erosion.

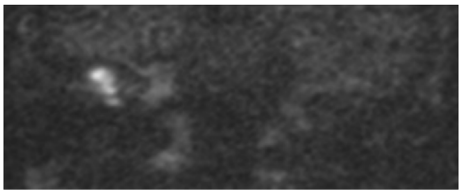

Fig. 1. Coronal b1000 image on DWMRI showing cholesteatoma in Prussak's space.

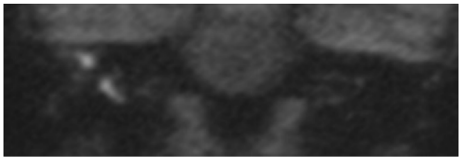

Fig. 2. Coronal b1000 image on DWMRI showing cholesteatoma extending into sinus tympani.

With DWMRI, a confident diagnosis of cholesteatoma was made (score 5) with high signal on b0 and b1000 images and low signal on ADC map.

On the fusion images, a confident diagnosis of cholesteatoma (score 5) was made by presence of high b1000 signal in the subsite clearly defined by bony anatomy of CT. This was then compared to the gold standard of surgical findings using the operative record (0 = cholesteatoma absent, 1 = cholesteatoma present).

In order to compare between the three imaging methods a bootstrapping approach was used. Analyses examined the diagnostic performance of each method compared to the gold standard method of surgery. Only data from the first observer was used in these analyses. For the diagnostic performance analyses, a result of ‘possible cholesteatoma’ or higher was assumed to be a ‘positive’ result with the remaining results considered negative. The diagnostic performance of each method was assessed by calculating the sensitivity, specificity and overall accuracy of the methods. Along with the calculated values, the uncertainty in the estimates was illustrated by calculating corresponding confidence intervals, using the exact binomial method. The paired exact test was used to compare diagnostic performance between each pair of imaging methods. All analyses were performed for each anatomical subsite separately, and then for all subsites combined [13].

Agreement in the assessments between the two observers was assessed using the weighted kappa method due to the ordinal nature of the outcome scale.

3. Results

Twenty-two patients were included (12 women and 10 men). The median age of patients was 11 years (range 6–18 years). The median gap between imaging and surgical intervention was 4 months (range 2–10 months). There was no significant relation between accuracy and gap between imaging and surgical intervention ($p = 1.00$).

3.1. Sensitivity

A summary of the sensitivity values for each modality is summarised in Table 1. The results suggested that, when all subsites were examined together, all methods had relatively high sensitivity values, all above 80% (87% for CT vs 84% for DWMRI vs 85% for fusion CT-DWMRI). Table 2 shows no significant differences in sensitivity between the three imaging methods.

3.2. Specificity

Table 3 shows the specificities of the three methods. The results

Table 1
Summary of the sensitivity values for each modality. The figures are the figures that the calculations were based on, along with calculated values and corresponding confidence intervals. The sensitivity values are expressed as a percentage.

Subsite	CT		DWMRI		Fusion	
	n/N	% (95% CI)	n/N	% (95% CI)	n/N	% (95% CI)
Epitympanum	14/15	93 (68, 100)	11/15	73 (45, 92)	12/15	80 (52, 96)
Aditus	10/11	91 (59, 100)	11/11	100 (72, 100)	11/11	100 (72, 100)
Prussak's	8/9	89 (52, 100)	9/9	100 (66, 100)	9/9	100 (66, 100)
Facial recess	10/11	91 (59, 100)	9/11	82 (48, 98)	9/11	82 (48, 98)
Sinus tympani	7/7	100 (59, 100)	6/7	86 (42, 100)	5/7	71 (29, 96)
Eustachian	6/11	55 (23, 83)	9/11	82 (48, 98)	8/11	73 (39, 94)
Facial nerve	0/3	0 (0, 71)	1/3	33 (1, 91)	2/3	67 (9, 99)
Hypotympanum	7/8	88 (47, 100)	7/8	88 (47, 100)	7/8	88 (47, 100)
Medial to Oss.	13/14	93 (66, 100)	13/14	93 (66, 100)	13/14	93 (66, 100)
Lateral to Oss.	14/15	93 (68, 100)	12/15	80 (52, 96)	13/15	87 (60, 98)
Mastoid	10/10	100 (69, 100)	8/10	80 (44, 97)	8/10	80 (44, 97)
All combined	99/114	87 (79, 92)	96/114	84 (76, 90)	97/114	85 (77, 91)

suggested typically low specificity values for the CT method (46% when all subsites were combined). This is primarily due to the method overestimating the proportion of patients with cholesteatoma. Specificity was typically higher for DWMRI (76% when all subsites were combined), and extremely high for the fusion CT-DWMRI method (97% when all subsites were combined). Table 4 shows that there were significant differences in specificity between all three imaging methods when all subsites were combined. The fusion CT-DWMRI method gave significantly higher specificity values than both DWMRI and CT, whilst DWMRI had significantly higher specificity values than fusion CT-DWMRI. There were a number of significant results for individual subsites, most notably between fusion CT-DWMRI and CT. Fusion CT-DWMRI had significantly higher specificity values than CT for 7 of the 11 subsites.

3.3. Accuracy

Table 5 shows the overall accuracy of the imaging methods. When all subsites were combined, accuracy was high for the fusion CT-DWMRI method (91%). This was lower for DWMRI (80%) and lower still for CT, which had only 66% accuracy. Table 6 shows significant differences in accuracy between each pair of imaging methods when the data from all subsites was combined. Fusion CT-DWMRI had significant higher accuracy than both DWMRI and CT, whilst DWMRI had significant higher accuracy than CT. There was significantly higher accuracy of fusion compared to CT in five of the individual subsites. There was no strong evidence of a difference in accuracy in individual subsites between fusion CT-DWMRI and DWMRI. However, there was evidence of a higher accuracy for the sinus tympani and hypotympanum subsites with fusion CT-DWMRI, although the differences did not quite reach statistical significance.

3.4. Agreement

Table 7 shows the agreement between the two observers using the weighted kappa method. The results for individual subsites suggested agreement ranging from poor (CT at facial nerve subsite) up to very good (DWMRI at aditus subsite). When considering all subsites combined, the result for all imaging methods suggested 'good' agreement between observers.

4. Discussion

Our study has demonstrated that fusion CT-DWMRI images are superior to DWMRI or CT separately in locating cholesteatoma at the various anatomical subsites in the middle ear cleft. The accuracy for fusion CT-DWMRI was significantly higher than that for DWMRI or CT. There was also good interobserver agreement in localizing the cholesteatoma. By providing a better map of the cholesteatoma in relation to the bony anatomy of the middle ear cleft, fusion CT-DWMRI paves the way for improved pre-operative counselling to patients about the extent of and surgical options for their disease. For the surgeon, it promotes better planning of surgery, e.g. clearing disease around the ossicles.

The primary advantage of fusion of CT-DWMRI is that it allows the MR-hyperintense cholesteatoma to be superimposed onto the bony anatomical details that can only be found on CT imaging, and this has

Table 2
Comparisons of the sensitivity between methods. The figures are the estimated difference in sensitivity between methods and a corresponding confidence interval. P-values indicating the significance of the differences between modalities are also reported.

Subsite	DWMRI - CT		Fusion - CT		Fusion - DWMRI	
	Diff (95% CI)	P	Diff (95% CI)	P	Diff (95% CI)	P
Epitympanum	−20 (−54, 14)	0.38	−13 (−45, 19)	0.63	7 (−13, 26)	1.00
Aditus	9 (−17, 35)	1.00	9 (−17, 35)	1.00	0 (−9, 9)	1.00
Prussak's	11 (−21, 43)	1.00	11 (−21, 42)	1.00	0 (−11, 11)	1.00
Facial recess	−9 (−35, 17)	1.00	−9 (−35, 17)	1.00	0 (−34, 34)	1.00
Sinus tympani	−14 (−54, 26)	1.00	−29 (−76, 19)	0.50	−14 (−54, 26)	1.00
Eustachian	27 (−8, 63)	0.25	18 (−14, 50)	0.50	−9 (−35, 17)	1.00
Facial nerve	33 (−53, 100)	1.00	67 (−20, 100)	0.50	33 (−53, 100)	1.00
Hypotympanum	0 (−47, 47)	1.00	0 (−47, 47)	1.00	0 (−47, 47)	1.00
Medial to Oss.	0 (−7, 7)	1.00	0 (−7, 7)	1.00	0 (−7, 7)	1.00
Lateral to Oss.	−13 (−45, 19)	0.63	−7 (−36, 22)	1.00	7 (−13, 26)	1.00
Mastoid	−20 (−55, 15)	0.50	−20 (−55, 15)	0.50	0 (−10, 10)	1.00
All combined	−3 (−11, 6)	0.66	−2 (−10, 7)	0.82	1 (−5, 7)	1.00

Table 3
Summary of the specificity values for each modality. The figures are the figures that the calculations were based on, along with calculated values and corresponding confidence intervals. The specificity values are expressed as a percentage.

Subsite	CT		DWMRI		Fusion	
	n/N	% (95% CI)	n/N	% (95% CI)	n/N	% (95% CI)
Epitympanum	1/7	14 (0, 58)	6/7	86 (42, 100)	7/7	100 (59, 100)
Aditus	7/11	64 (31, 89)	11/11	100 (72, 100)	11/11	100 (72, 100)
Prussak's	3/13	23 (5, 54)	11/13	85 (55, 98)	13/13	100 (75, 100)
Facial recess	4/11	36 (11, 69)	7/11	64 (31, 89)	11/11	100 (72, 100)
Sinus tympani	5/15	33 (12, 62)	8/15	53 (27, 79)	15/15	100 (78, 100)
Eustachian	4/11	36 (11, 69)	7/11	64 (31, 89)	9/11	82 (48, 98)
Facial nerve	18/19	95 (74, 100)	18/19	95 (74, 100)	18/19	95 (74, 100)
Hypotympanum	6/14	43 (18, 71)	8/14	57 (29, 82)	14/14	100 (77, 100)
Medial to Oss.	2/8	25 (3, 65)	6/8	75 (35, 97)	8/8	100 (63, 100)
Lateral to Oss.	1/7	14 (0, 58)	4/7	57 (18, 90)	7/7	100 (59, 100)
Mastoid	8/12	67 (35, 90)	11/12	92 (62, 100)	11/12	92 (62, 100)
All combined	59/128	46 (37, 55)	97/128	76 (67, 83)	124/128	97 (92, 99)

Table 4
Comparisons of the specificity between methods. The figures are the estimated difference in specificity between methods and a corresponding confidence interval. P-values indicating the significance of the differences between modalities are also reported.

Subsite	DWMRI - CT		Fusion - CT		Fusion - DWMRI	
	Diff (95% CI)	P	Diff (95% CI)	P	Diff (95% CI)	P
Epitympanum	71 (5, 100)	0.13	86 (46, 100)	**0.03**	14 (−26, 54)	1.00
Aditus	36 (−1, 74)	0.13	36 (−1, 74)	0.13	0 (−9, 9)	1.00
Prussak's	62 (20, 100)	**0.02**	77 (46, 100)	**0.002**	15 (−12, 43)	0.50
Facial recess	27 (−18, 73)	0.38	64 (26, 100)	**0.02**	36 (−1, 74)	0.13
Sinus tympani	20 (−14, 54)	0.38	−29 (−76, 19)	**0.002**	47 (15, 79)	**0.02**
Eustachian	27 (−18, 73)	0.38	45 (−2, 93)	0.13	18 (−14, 50)	0.50
Facial nerve	0 (−20, 20)	1.00	0 (−5, 5)	1.00	0 (−20, 20)	1.00
Hypotympanum	14 (−26, 55)	0.69	57 (24, 90)	**0.008**	43 (10, 76)	**0.03**
Medial to Oss.	50 (−11, 100)	0.22	75 (32, 100)	**0.03**	25 (−18, 68)	0.50
Lateral to Oss.	43 (−25, 100)	0.38	86 (46, 100)	**0.03**	43 (−8, 94)	0.25
Mastoid	25 (−8, 58)	0.25	25 (−8, 58)	0.25	0 (−8, 8)	1.00
All combined	30 (18, 41)	< **0.001**	51 (41, 60)	< **0.001**	21 (13, 29)	< **0.001**

been demonstrated previously [10]. It is a post-processing process and does not require any further imaging than that would be performed anyway. There is no additional cost or radiation exposure. Fusion of CT and DWMRI is relatively straight forward, taking some extra time post-acquisiton (approximately 20 min in our study) with both automatic and manual registration of the images. However, with advances in software techniques, this process could be quicker and more straightforward. Incorporating this technique through surgical navigation software will be of particular value in guiding surgery in skull base surgery, as has been described previously for anterior skull base surgery [14].

Although non-echoplanar DWMRI has been shown to accurately localise cholesteatoma in various middle ear subsites, fusion CT-DWMRI has the additional advantage of localizing cholesteatoma in relation to precise bony structures such as the facial nerve canal and ossicles [2,15]. Demonstrating the relations of the disease in relation to

Table 5
Summary of the accuracy values for each modality. The figures are the figures that the calculations were based on, along with calculated values and corresponding confidence intervals. The accuracy values are expressed as a percentage.

Subsite	CT		DWMRI		Fusion	
	n/N	% (95% CI)	n/N	% (95% CI)	n/N	% (95% CI)
Epitympanum	15/22	68 (45, 86)	17/22	77 (55, 92)	19/22	86 (65, 97)
Aditus	17/22	77 (55, 92)	22/22	100 (85, 100)	22/22	100 (85, 100)
Prussak's	11/22	50 (28, 72)	20/22	91 (71, 99)	22/22	100 (85, 100)
Facial recess	14/22	64 (41, 83)	16/22	72 (50, 89)	20/22	91 (71, 99)
Sinus tympani	12/22	55 (32, 76)	14/22	64 (41, 83)	20/22	91 (71, 99)
Eustachian	10/22	45 (24, 68)	16/22	73 (50, 89)	17/22	77 (55, 92)
Facial nerve	18/22	81 (60, 95)	19/22	86 (65, 97)	20/22	91 (71, 99)
Hypotympanum	13/22	59 (36, 79)	15/22	68 (45, 86)	21/22	95 (77, 100)
Medial to Oss.	15/22	68 (45, 86)	19/22	86 (65, 97)	21/22	95 (77, 100)
Lateral to Oss.	15/22	68 (45, 86)	16/22	73 (50, 89)	20/22	91 (71, 99)
Mastoid	18/22	82 (60, 95)	19/22	86 (65, 97)	19/22	86 (65, 97)
All combined	158/242	66 (59, 71)	193/242	80 (74, 85)	221/242	91 (87, 95)

Table 6
Comparisons of the accuracy between methods. The figures are the estimated difference in accuracy between methods and a corresponding confidence interval. P-values indicating the significance of the differences between modalities are also reported.

Subsite	DWMRI - CT		Fusion - CT		Fusion – DWMRI	
	Diff (95% CI)	P	Diff (95% CI)	P	Diff (95% CI)	P
Epitympanum	9 (−26, 44)	0.77	18 (−13, 50)	0.34	9 (−7, 26)	0.50
Aditus	23 (1, 45)	0.06	23 (1, 45)	0.06	0 (−5, 5)	1.00
Prussak's	41 (12, 70)	**0.01**	50 (25, 75)	**0.001**	9 (−7, 26)	0.50
Facial recess	9 (−17, 35)	0.69	27 (0, 54)	0.07	18 (−7, 43)	0.22
Sinus tympani	9 (−17, 35)	0.69	36 (5, 68)	**0.04**	27 (0, 54)	0.07
Eustachian	27 (0, 54)	0.07	32 (4, 60)	**0.04**	5 (−15, 24)	1.00
Facial nerve	5 (−15, 24)	1.00	9 (−7, 26)	0.50	5 (−15, 24)	1.00
Hypotympanum	9 (−20, 39)	0.73	36 (8, 65)	**0.02**	27 (0, 54)	0.07
Medial to Oss.	18 (−7, 43)	0.22	27 (4, 50)	**0.03**	9 (−7, 26)	0.50
Lateral to Oss.	5 (−27, 36)	1.00	23 (−7, 52)	0.18	18 (−2, 39)	0.13
Mastoid	5 (−20, 29)	1.00	5 (−20, 29)	1.00	0 (−5, 5)	1.00
All combined	14 (7, 22)	< **0.001**	26 (19, 33)	< **0.001**	12 (6, 17)	< **0.001**

Table 7
Summary of the kappa values for each anatomical subsite separately, and combined. The figures are the calculated kappa values, along with corresponding confidence intervals.

Subsite	CT Kappa (95% CI)	DWMRI Kappa (95% CI)	Fusion Kappa (95% CI)
Epitympanum	0.67 (0.37, 0.97)	0.81 (0.47, 1.00)	0.82 (0.42, 1.00)
Aditus	0.81 (0.52, 1.00)	0.95 (0.55, 1.00)	0.91 (0.51, 1.00)
Prussak's space	0.73 (0.45, 1.00)	0.72 (0.37, 1.00)	0.88 (0.50, 1.00)
Facial recess	0.37 (0.08, 0.65)	0.55 (0.24, 0.85)	0.57 (0.26, 0.88)
Sinus tympani	0.28 (−0.01, 0.56)	0.58 (0.28, 0.88)	0.49 (0.15, 0.83)
Eustachian	0.72 (0.40, 1.00)	0.66 (0.32, 1.00)	0.48 (0.15, 0.81)
Facial nerve	0.07 (−0.05, 0.20)	0.20 (0.00, 0.40)	0.18 (−0.11, 0.47)
Hypotympanum	0.76 (0.42, 1.00)	0.71 (0.37, 1.00)	0.55 (0.22, 0.89)
Medial to Ossicles	0.59 (0.26, 0.91)	0.71 (0.37, 1.00)	0.95 (0.54, 1.36)
Lateral to Ossicles	0.60 (0.28, 0.91)	0.78 (0.42, 1.00)	0.82 (0.45, 1.00)
Mastoid	0.55 (0.28, 0.81)	0.79 (0.43, 1.00)	0.52 (0.41, 1.00)
All combined	0.61 (0.53, 0.70)	0.72 (0.62, 0.82)	0.76 (0.65, 0.87)

the facial nerve canal and assessing for canal erosion is of paramount importance when excising cholesteatoma in this region, as it dictates whether there is bony covering over the facial nerve, and can therefore be useful in surgical planning for dissection over this critical area. However, even CT does not have 100% accuracy in determining whether the facial nerve is dehiscent, particularly in the tympanic segment. Fusion CT-DWMRI also is particularly useful to identify disease medial to the ossicles, which can help to avoid unnecessary removal of the ossicles if there is no disease medial to the ossicles, and therefore prevent potential hearing loss post-operatively.

Our study has demonstrated the value of fusion CT-DWMRI over CT or DWMRI individually in identifying cholesteatoma medial to the ossicles, facial nerve involvement and erosion, and in identifying disease in the Eustachian tube orifice and hypotympanum, areas where surgical access can be difficult. Fig. 3 demonstrates the particular benefit of fusion imaging identifying cholesteatoma medial to the ossicles, which

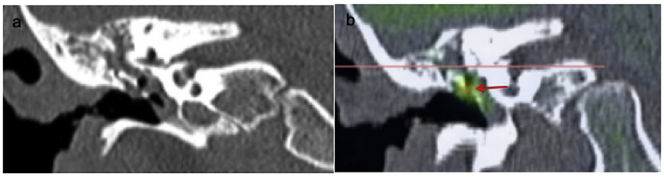

Fig. 3. Coronal images show cholesteatoma (red arrow) medial to the ossicles with high confidence (score 5) on the fused image (b) but this is not confidently depicted (score 3) on CT (a). (For interpretation of the references to colour in this figure legend, the reader is referred to the Web version of this article.)

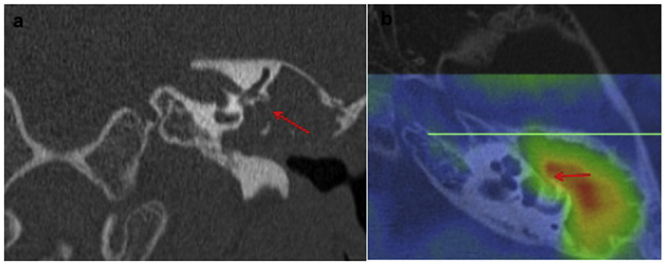

Fig. 4. (a) Coronal CT show disease possibly eroding facial nerve canal (confidence score 3) (red arrow). (b) Axial fusion image shows confidently (score 5) disease in the region of the canal. (For interpretation of the references to colour in this figure legend, the reader is referred to the Web version of this article.)

wasn't identified on CT or DWMRI. This is useful from a practical perspective as it allows the clinician to counsel the patient pre-operatively regarding the need to remove the ossicles intra-operatively, resulting in hearing impairment. Fig. 4 demonstrates the benefit of fusion CT-DWMRI imaging over CT in identifying facial nerve involvement and erosion, as fusing the CT and DWMRI images allows more accurate localisation of the disease. Fig. 5 highlights the superiority of fusion CT-DWMRI in identifying cholesteatoma in the Eustachian tube orifice and hypotympanum when compared to CT and DWMRI individually. This can guide planning of surgery regarding the extent of disease.

Several false negative cases for cholesteatoma in various subsites were noted on fusion CT-DWMRI. Although non-EPI DWMRI is highly accurate in detecting middle ear cleft cholesteatoma, previous studies have identified its limitations in identifying small volume of disease typically less than 2–3 mm [2,16–19]. Our study demonstrates that this limitation in sensitivity is inherent in the performance of fusion CT-

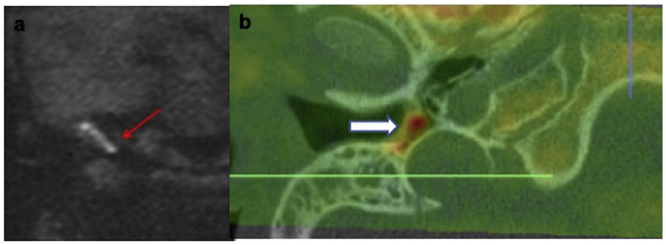

Fig. 5. (a) Coronal b1000 image show right cholesteatoma (red arrow) but it is unclear if it is involving the hypotympanum - confidence score 3 (b) axial fusion image shows confidently (score 5) disease in hypotympanum and eustachian tube orifice with added bony anatomy detail. (For interpretation of the references to colour in this figure legend, the reader is referred to the Web version of this article.)

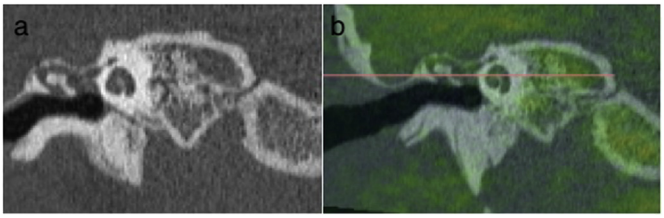

Fig. 6. (a) Coronal CT and (b) fusion images and DWMRI (not shown) all did not confidently detect the small cholesteatoma at the anterior epitympanum.

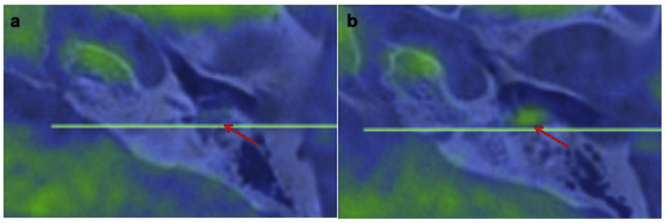

Fig. 7. Axial fusion image did not detect cholesteatoma at the sinus tympani/facial recess (a). The cholesteatoma (b) was located slightly cranial to this area due to slight misregistration.

DWMRI by 2 cases of small volume disease in the anterior epitympanum and lateral to the ossicles which were not depicted on fusion CT-DWMRI (Fig. 6). On surgery they were attic retraction harbouring a small focus of disease. In both these cases this represented recurrent disease, as opposed to residual disease. DWMRI in assessing cholesteatoma in retraction pockets is known to be an area of controversy. In another subsite, the Eustachian tube orifice, imaging (both CT, DWMRI and fusion CT-DWMRI) was unable to accurately localise cholesteatoma in one case when it was present intra-operatively. This could be because when cholesteatoma involves the Eustachian tube orifice it can form a thin layer on the wall, which may not be detectable on imaging. In two cases there was also some difficulty with identifying cholesteatoma present intra-operatively in the facial recess and sinus tympani on fusion imaging due to slight image slice misregistration during the fusion process (Fig. 7). Given that the facial recess and sinus tympani are such small and precise anatomical locations, fusion imaging may have significant effects on accuracy in these locations but this may be improved by training, experience and advances in fusion technology.

Our study has demonstrated that fusion CT-DWMRI has high accuracy for localizing cholesteatoma in the middle ear cleft. It reinforces previously published studies to include a smaller feasibility study from Japan of 12 patients which demonstrated accurate correlation between fusion CT-DWMRI and surgery for location and extent of cholesteatoma [20]. Another recent study of 12 patients that looked at the accuracy of each imaging modality in cholesteatoma diagnosis and localisation across 6 distinct anatomical locations of the temporal bone, showed overall accuracy of 0.83 for DWMRI and 0.90 for fusion CT-DWMRI, which again compares favourably to our results [10]. Our results have demonstrated how potentially fusion imaging can be useful in pre-operative planning and can modify surgical approach (e.g. combined approach tympanomastoidectomy versus 'inside out' tympanomastoidectomy). This has been demonstrated in a study that looked at the use fusion CT-DWMRI in a population of 10 children. They concluded that 3 patients had their surgical approach modified based on review of the fused images pre-operatively [21]. In the post-operative setting to evaluate for recurrent or residual disease, a recent prospective study of 28 patients demonstrated that preoperative CT scans before the first operation can be used with post-operative non-EPI DWMRI to accurately detect and localise residual cholesteatoma, thus sparing patients unnecessary radiation exposure from further CT scanning [11]. Total endoscopic ear surgery is increasingly gaining favour as the advantages of improved visualisation and less morbidity with the endoscopic approach versus the open approach for cholesteatoma surgery are well documented [22]. A previously published paper has reported the advantage of fusion CT-DWMRI in determining whether patients are appropriate for transcanal endoscopic ear surgery, due to the reliable diagnostic accuracy of fusion CT-DWMRI in identifying the anatomical location of cholesteatoma [23].

Fusion CT-DWMRI incorporates the limitations of non-EPI DWMRI including its slight lack of specificity. Whilst restriction of water molecules is important in generating high signal on DWMRI, a 'T2 shine-through' effect (high signal in tissues that have prolonged T2 relaxation) has been proposed as one theory for the high signal [24]. Though not encountered in our small study, some substances that have prolonged T2 relaxation potential, and can thus cause false positives, include cerumen, proteinaceous inflammation/fluid, silastic sheets and occasional cartilage grafts [24–26]. Even though the false positive DWMRI signal can be mitigated with the use of T1W MRI images as part of the MRI protocol and interpretation, this correction is not inherent in the fused images [27,28] and may need to be interpreted with T1W images for better accuracy.

By blinding the two independent head and neck radiologists to the results and using confidence scoring, as well as using the surgical findings as the gold standard for the anatomical location of cholesteatoma, we have strengthened the reliability of this study. However, there was a limited sample size, and there are limitations in the accuracy of operative records in terms of the anatomical location of cholesteatoma. The analyses suggested some differences between imaging modalities for all subsites combined, but fewer differences for individual subsites. This is likely to be due to the much smaller amount of data, and thus lack of statistical power, for subsites separately. This is particularly the case for the sensitivity and specificity analyses which do not use all data in the analyses. Further larger prospective studies, preferably randomised control trials, are required to validate our findings.

5. Conclusion

Within the limits of our study, we have demonstrated that fusion CT-DWMRI is considerably superior to DWMRI or CT separately in terms of accurately locating cholesteatoma to various middle ear subsites and bony structures, by allowing the DWMRI-hyperintense b1000 signal cholesteatoma to be superimposed onto the bony anatomical details that can only be found on high resolution CT imaging. This is of particular value in guiding surgical planning.

6. Summary

- Diagnosis of cholesteatoma is usually clinical and management is surgical, but imaging can be helpful in determining extent of disease and in surgical planning.
- Whilst CT is useful in demonstrating bony anatomy and soft tissue, it has limitations in differentiating granulation tissue and cholesteatoma.
- DWMRI is a more specific imaging modality for cholesteatoma, but it has poor anatomical spatial resolution, thus limiting localisation of cholesteatoma.
- The primary advantage of fusion CT-DWMRI is that it allows the MR-hyperintense cholesteatoma to be superimposed onto the bony anatomical details that can only be found on CT imaging.
- Our data has demonstrated that fusion of DWMRI and CT images performs better than DWMRI or CT separately, with good inter-observer agreement, in localizing cholesteatoma to various middle ear cleft subsites and bony structures, bestowing it particular value in surgical planning.

Financial support

This research received no specific grant from any funding agency,

commercial or not-for-profit sectors.

Declaration of competing interest

None.

Acknowledgements

Grateful thanks to Paul Bassett for his help with statistical analysis, and to the administrative staff in the ENT Department in Northwick Park Hospital.

References

[1] R. Lingam, P. Bassett, A meta-analysis on the diagnostic performance of non-echoplanar diffusion-weighted imaging in detecting middle ear cholesteatoma: 10 Years on, Otol. Neurotol. 38 (4) (2017) 521–528.
[2] A. Majithia, R.K. Lingam, R. Nash, S. Khemani, A. Kalan, A. Singh, Staging primary middle ear cholesteatoma with non-echoplanar (half-Fourier-acquisition single-shot turbo-spin-echo) diffusion-weighted magnetic resonance imaging helps plan surgery in 22 patients: our experience, Clin. Otolaryngol. 37 (4) (2012) 325–330.
[3] N.W. Chee, T.Y. Tan, The value of pre-operative high resolution CT scans in cholesteatoma surgery, Singap. Med. J. 42 (4) (2001) 155–159.
[4] P.A. Tierney, P. Pracy, S.P. Blaney, D.A. Bowdler, An assessment of the value of the preoperative computed tomography scans prior to otoendoscopic 'second look' in intact canal wall mastoid surgery, Clin. Otolaryngol. Allied Sci. 24 (4) (1999) 274–276.
[5] C.T. Huins, A. Singh, R.K. Lingam, A. Kalan, Detecting cholesteatoma with non-echo planar (HASTE) diffusion-weighted magnetic resonance imaging, Otolaryngol. Head Neck Surg. 143 (1) (2010) 141–146.
[6] R.K. Lingam, P. Khatri, J. Hughes, A. Singh, Apparent diffusion coefficients for detection of postoperative middle ear cholesteatoma on non-echo-planar diffusion-weighted images, Radiology 269 (2) (2013) 504–510.
[7] K.M. Schwartz, J.I. Lane, B.D. Bolster Jr., B.A. Neff, The utility of diffusion-weighted imaging for cholesteatoma evaluation, AJNR Am. J. Neuroradiol. 32 (3) (2011) 430–436.
[8] S.L. van Egmond, I. Stegeman, W. Grolman, M.C. Aarts, A systematic review of non-echo planar diffusion-weighted magnetic resonance imaging for detection of primary and postoperative cholesteatoma, Otolaryngol. Head Neck Surg. 154 (2) (2016) 233–240.
[9] J. Muzaffar, C. Metcalfe, S. Colley, C. Coulson, Diffusion-weighted magnetic resonance imaging for residual and recurrent cholesteatoma: a systematic review and meta-analysis, Clin. Otolaryngol. 42 (3) (2017) 536–543.
[10] G.D. Locketz, P.M. Li, N.J. Fischbein, S.J. Holdsworth, N.H. Blevins, Fusion of computed tomography and PROPELLER diffusion-weighted magnetic resonance imaging for the detection and localization of middle ear cholesteatoma, JAMA Otolaryngol. Head Neck Surg. 142 (10) (2016) 947–953.
[11] M. Alzahrani, R. Alhazmi, M. Bélair, I. Saliba, Postoperative diffusion weighted MRI and preoperative CT scan fusion for residual cholesteatoma localization, Int. J. Pediatr. Otorhinolaryngol. 90 (2016) 259–263.
[12] R.K. Lingam, S.E.J. Connor, J.W. Casselman, T. Beale, MRI in otology: applications in cholesteatoma and Ménière's disease, Clin. Radiol. 73 (1) (2018) 35–44.
[13] https://www.graphpad.com/scientific-software/prism/ , Accessed date: 2 May 2018.
[14] O. Francies, L. Makalanda, D. Paraskevopolous, A. Adams, Imaging review of the anterior skull base, Acta Radiol. Open 7 (5) (2018) 2058460118776487.
[15] S. Khemani, R.K. Lingam, A. Kalan, A. Singh, The value of non-echo planar HASTE diffusion-weighted MR imaging in the detection, localisation and prediction of extent of postoperative cholesteatoma, Clin. Otolaryngol. 36 (4) (2011) 306–312.
[16] B. De Foer, J.P. Vercruysse, A. Bernaerts, J. Maes, F. Deckers, J. Michiels, T. Somers, M. Pouillon, E. Offeciers, J.W. Casselman, The value of single-shot turbo spin-echo diffusion-weighted MR imaging in the detection of middle ear cholesteatoma, Neuroradiology 49 (10) (2007) 841–848.
[17] K. Baráth, A.M. Huber, P. Stämpfli, Z. Varga, S. Kollias, Neuroradiology of cholesteatomas, AJNR Am. J. Neuroradiol. 32 (2) (2011) 221–229.
[18] R. Nash, P.Y. Wong, A. Kalan, R.K. Lingam, A. Singh, Comparing diffusion weighted MRI in the detection of post-operative middle ear cholesteatoma in children and adults, Int. J. Pediatr. Otorhinolaryngol. 79 (12) (2015) 2281–2285.
[19] R. Nash, A. Kalan, R.K. Lingam, A. Singh, The role of diffusion-weighted magnetic resonance imaging in assessing residual/recurrent cholesteatoma after canal wall down mastoidectomy, Clin. Otolaryngol. 41 (3) (2016) 307–309.
[20] K. Yamashita, A. Hiwatashi, O. Togao, K. Kikuchi, N. Matsumoto, M. Obara, T. Yoshiura, H. Honda, High-resolution three-dimensional diffusion-weighted MRI/CT image data fusion for cholesteatoma surgical planning: a feasibility study, Eur. Arch. Oto-Rhino-Laryngol. 272 (12) (2015) 3821–3824.
[21] I. Plouin-Gaudon, D. Bossard, S. Ayari-Khalfallah, P. Froehlich, Fusion of MRIs and CT scans for surgical treatment of cholesteatoma of the middle ear in children, Arch. Otolaryngol. Head Neck Surg. 136 (9) (2010) 878–883.
[22] C.P. Yiannakis, R. Sproat, A. Iyer, Preliminary outcomes of endoscopic middle-ear surgery in 103 cases: a UK experience, J. Laryngol. Otol. 132 (6) (2018 Jun) 493–496.
[23] T. Watanabe, T. Ito, T. Furukawa, K. Futai, T. Kubota, M. Kanoto, Y. Toyoguchi, T. Hosoya, S. Kakehata, The efficacy of color-mapped diffusion-weighted images combined with CT in the diagnosis and treatment of cholesteatoma using transcanal endoscopic ear surgery, Otol. Neurotol. 36 (10) (2015) 1663–1668.
[24] M. Jindal, A. Riskalla, D. Jiang, S. Connor, A.F. O'Connor, A systematic review of diffusion-weighted magnetic resonance imaging in the assessment of postoperative cholesteatoma, Otol. Neurotol. 32 (8) (2011) 1243–1249.
[25] L. Migirov, M. Wolf, G. Greenberg, A. Eyal, Non-EPI DW MRI in planning the surgical approach to primary and recurrent cholesteatoma, Otol. Neurotol. 35 (1) (2014) 121–125.
[26] F. Venail, A. Bonafe, V. Poirrier, M. Mondain, A. Uziel, Comparison of echo-planar diffusion-weighted imaging and delayed postcontrast T1-weighted MR imaging for the detection of residual cholesteatoma, AJNR Am. J. Neuroradiol. 29 (7) (2008) 1363–1368.
[27] A. Fukuda, S. Morita, T. Harada, K. Fujiwara, K. Hoshino, Y. Nakamaru, A. Homma, Value of T1-weighted magnetic resonance imaging in cholesteatoma detection, Otol. Neurotol. 38 (10) (2017 Dec) 1440–1444.
[28] R.K. Lingam, R. Nash, A. Majithia, A. Kalan, A. Singh, Non-echoplanar diffusion weighted imaging in the detection of post-operative middle ear cholesteatoma: navigating beyond the pitfalls to find the pearl, Insights Imag. 7 (5) (2016 Oct) 669–678.